Supplementary Information

Ternary Alloy Nanocrystals of Tin and Germanium Chalcogenides

Hyung Soon Im, Yoon Myung, Kidong Park, Chan Su Jung, Young Rok Lim, Dong Myung Jang, and Jeunghee Park

Content

Table S1. Pressure of precursors in the closed reactor for the synthesis of NCs.

Composition	No.	x (Sn)	Pressure (Torr)			
			$Ge(CH_3)_4$	$Sn(CH_3)_4$	H_2S	$Se(CH_3)_2$
$Sn_xGe_{1-x}S$	1	0	20	0	40	0
	2	0.05	39	1	60	0
	3	0.12	38	2	60	0
	4	0.25	34	6	60	0
	5	0.42	30	10	60	0
	6	0.54	25	15	60	0
	7	0.57	22	18	60	0
	8	0.64	20	20	60	0
	9	0.70	17	23	60	0
	10	0.75	15	25	60	0
	11	0.85	12	28	60	0
	12	0.9	10	30	60	0
	13	0.97	4	36	60	0
	14	1	0	20	40	0
$Sn_xGe_{1-x}Se$	1	0	20	0	0	20
	2	0.06	19	1	0	20
	3	0.18	18	2	0	20
	4	0.31	17	3	0	20
	5	0.40	16	4	0	20
	6	0.52	15	5	0	20
	7	0.60	12	8	0	20
	8	0.72	10	10	0	20
	9	0.87	5	15	0	20
	10	0.95	3	17	0	20
	11	0.98	1	19	0	20
	12	1	0	20	0	20

Composition	No.	x (S)	Pressure (Torr)			
			$Ge(CH_3)_4$	$Sn(CH_3)_4$	H_2S	$Se(CH_3)_2$
GeS_xSe_{1-x}	1	0	20	0	0	20
	2	0.06	30	0	7	25
	3	0.07	30	0	8	22
	4	0.17	30	0	10	20
	5	0.25	25	0	20	20
	6	0.34	25	0	25	15
	7	0.38	30	0	20	10
	8	0.41	30	0	30	10
	9	0.46	25	0	25	07
	10	0.65	25	0	32	08
	11	0.76	25	0	35	05
	12	0.82	30	0	37	03
	13	0.85	30	0	39	01
	14	0.91	30	0	38	02
	15	1	20	0	40	0
SnS_xSe_{1-x}	1	0	0	30	0	30
	2	0.07	0	30	10	30
	3	0.12	0	30	15	25
	4	0.22	0	30	20	25
	5	0.31	0	30	20	20
	6	0.39	0	30	20	15
	7	0.42	0	30	25	15
	8	0.55	0	30	34	15
	9	0.57	0	30	30	10
	10	0.60	0	30	40	10
	11	0.73	0	30	45	5
	12	0.79	0	30	34	6
	13	0.82	0	30	38	2
	14	0.91	0	30	39	1
	15	1	0	30	50	0

Table S2. The onset of absorption band and indirect/direct band gaps estimated from its K-M transformation.

Composition	x	Onset (eV)	Indirect band gap (eV)	Direct band gap (eV)
$Sn_xGe_{1-x}S$	0	1.59	1.57	1.58
	0.05	1.57	1.55	1.53
	0.12	1.48	1.48	1.50
	0.25	1.40	1.40	1.43
	0.42	1.37	1.35	1.39
	0.54	1.33	1.32	1.33
	0.57	1.33	1.32	1.33
	0.64	1.31	1.30	1.32
	0.70	1.31	1.29	1.33
	0.75	1.29	1.27	1.31
	0.85	1.25	1.24	1.27
	0.90	1.23	1.22	1.24
	0.97	1.23	1.22	1.25
	1	1.25	1.23	1.25
$Sn_xGe_{1-x}Se$	0	1.20	1.20	1.20
	0.06	1.20	1.19	1.21
	0.18	1.16	1.15	1.16
	0.31	1.08	1.07	1.08
	0.40	1.05	1.05	1.05
	0.52	1.03	1.03	1.03
	0.60	0.99	0.99	1.0
	0.72	0.96	0.95	0.96
	0.87	0.93	0.92	0.93
	0.94	0.90	0.90	0.90
	0.98	0.92	0.91	0.92
	1	0.92	0.92	0.92
GeS_xSe_{1-x}	0	1.20	1.20	1.20
	0.06	1.22	1.22	1.22
	0.07	1.23	1.23	1.24
	0.17	1.24	1.24	1.24
	0.25	1.27	1.27	1.26
	0.34	1.31	1.31	1.31
	0.38	1.35	1.35	1.35
	0.41	1.39	1.37	1.39

	0.46	1.42	1.40	1.41
	0.65	1.44	1.44	1.44
	0.76	1.47	1.47	1.48
	0.82	1.52	1.52	1.52
	0.85	1.56	1.56	1.56
	0.91	1.57	1.56	1.57
	1	1.59	1.57	1.57
SnS$_x$Se$_{1-x}$	0	0.92	0.92	0.92
	0.07	0.93	0.94	0.94
	0.12	0.98	0.98	0.98
	0.22	0.97	0.98	0.99
	0.31	1.00	1.00	1.01
	0.39	1.02	1.02	1.03
	0.42	1.04	1.04	1.04
	0.55	1.08	1.08	1.09
	0.57	1.11	1.10	1.10
	0.60	1.13	1.13	1.14
	0.73	1.16	1.15	1.15
	0.79	1.16	1.16	1.15
	0.82	1.21	1.20	1.19
	0.91	1.20	1.20	1.19
	1	1.25	1.23	1.25

Table S3. Position of conduction and valence bands (in eV) versus vacuum level, which were estimated from the CV and UV-Vis-NIR absorption spectroscopy data.

Composition	x (Sn)	E_{Ox}(eV)[a]	E_{VB} (eV)[b]	E_g (eV)[c]	E_{CB} (eV)[d]
$Sn_xGe_{1-x}S$	0	0.48	-5.20	1.57	-3.63
	0.12	0.44	-5.16	1.48	-3.68
	0.25	0.38	-5.10	1.40	-3.70
	0.42	0.37	-5.09	1.35	-3.74
	0.57	0.33	-5.05	1.32	-3.73
	0.75	0.28	-5.00	1.27	-3.73
	0.90	0.25	-4.97	1.22	-3.75
	0.97	0.24	-4.96	1.22	-3.75
	1	0.29	-5.01	1.23	-3.78
$Sn_xGe_{1-x}Se$	0	0.36	-5.08	1.19	-3.89
	0.19	0.36	-5.08	1.15	-3.93
	0.52	0.35	-5.07	1.03	-4.04
	0.73	0.35	-5.07	0.96	-4.11
	0.87	0.33	-5.05	0.93	-4.12
	1	0.32	-5.04	0.92	-4.12

[a]Onset value of oxidation peak of CV curves (relative to the Ag/Ag$^+$ reference electrode); [b]E_{VB} = -(E_{Ox}+4.715) eV; [c]Indirect band gap, which is estimated from the K-M transformation of UV-visible-NIR absorption band; [d]E_{CB} (eV)= E_{VB}+ E_g.

Figure S1. XRD pattern of (a) $Sn_xGe_{1-x}S$ (x = 0, 0.1, 0.4, 0.6, 0.9, and 1), (b) $Sn_xGe_{1-x}Se$ (x = 0, 0.2, 0.5, 0.7, 0.9, and 1), (c) GeS_xSe_{1-x} (x = 0, 0.1, 0.3, 0.6, 0.8, and 1), and (d) SnS_xSe_{1-x} (x = 0, 0.2, 0.4, 0.6, 0.9, and 1) NCs. The (111) peak region, corresponding to 2θ = 29–35°, has been magnified to show the shift of the lattice constants upon varying the composition of the alloy.

For $Sn_xGe_{1-x}S$, the peaks of GeS and SnS were indexed to the orthorhombic phase with a *Pbmn* space group; GeS (JCPDS No. 85-1114, a = 4.290 Å, b = 10.42 Å, c = 3.640 Å) and SnS (JCPDS No. 39-0354; a = 4.329 Å, b = 11.19 Å, c = 3.983 Å). For $Sn_xGe_{1-x}Se$, the peaks of GeSe and SnSe were indexed to the orthorhombic phase with a *Pnma* space group; GeSe (JCPDS No. 48-1226; a = 10.84 Å, b = 3.834 Å, c = 4.390 Å) and SnSe (JCPDS No. 48-1224; a = 11.49 Å, b = 4.153 Å, c = 4.440 Å). The peaks of GeS_xSe_{1-x} were assigned to those of *Pbnm* space group; GeS (JCPDS No. 85-1114, a = 4.290 Å, b = 10.42 Å, c = 3.640 Å) and GeSe (JCPDS No. 33-0582; a = 4.3880 Å, b = 10.8250 Å, c = 3.8830 Å). The peaks of SnS_xSe_{1-x} were assigned to those of *Pnma* space group; SnS (JCPDS No. 73-1859; a = 11.18 Å, b = 3.982 Å, c = 4.329 Å) and SnSe (JCPDS No. 48-1224; a = 11.49 Å, b = 4.153 Å, c = 4.440 Å).
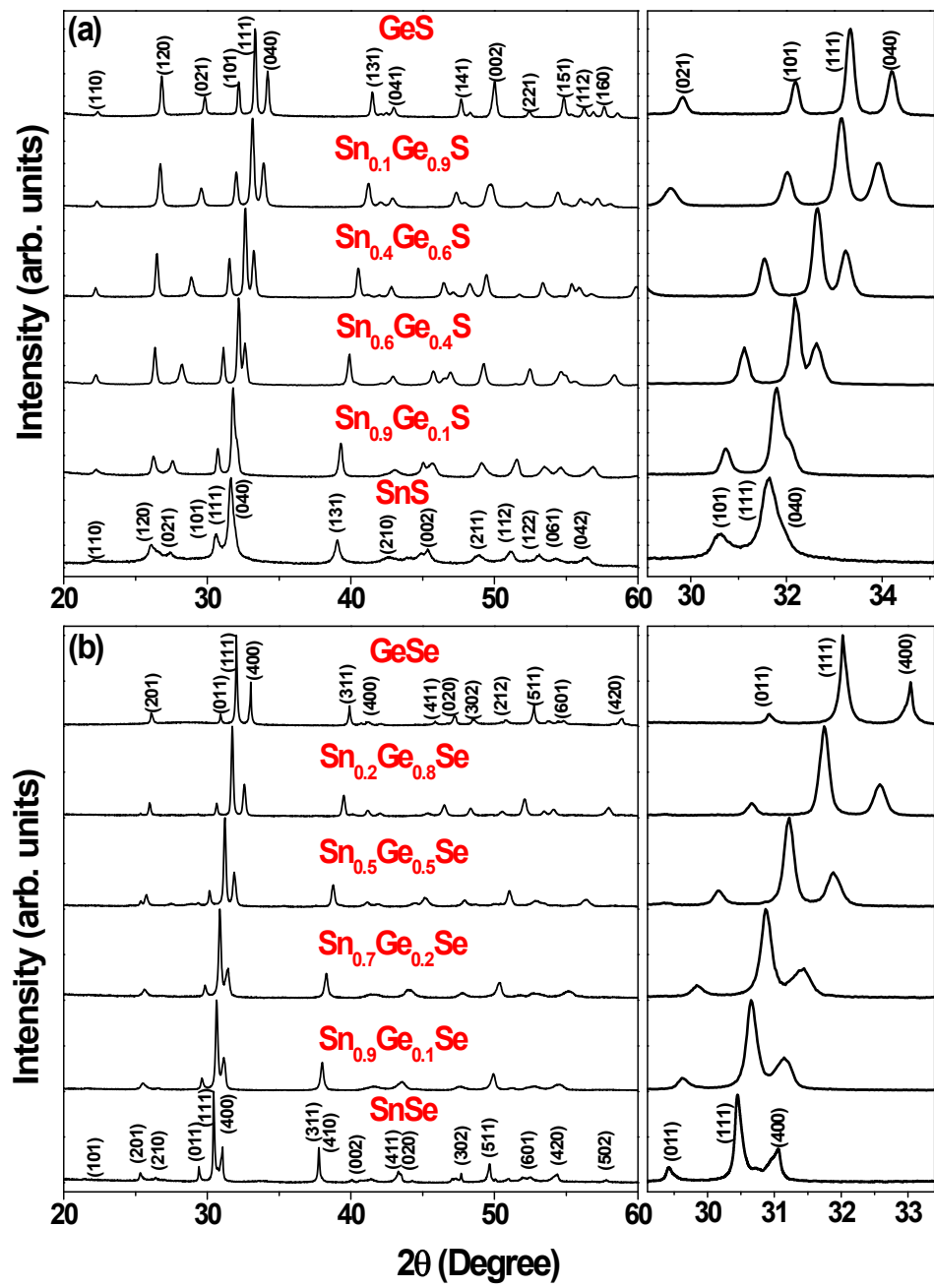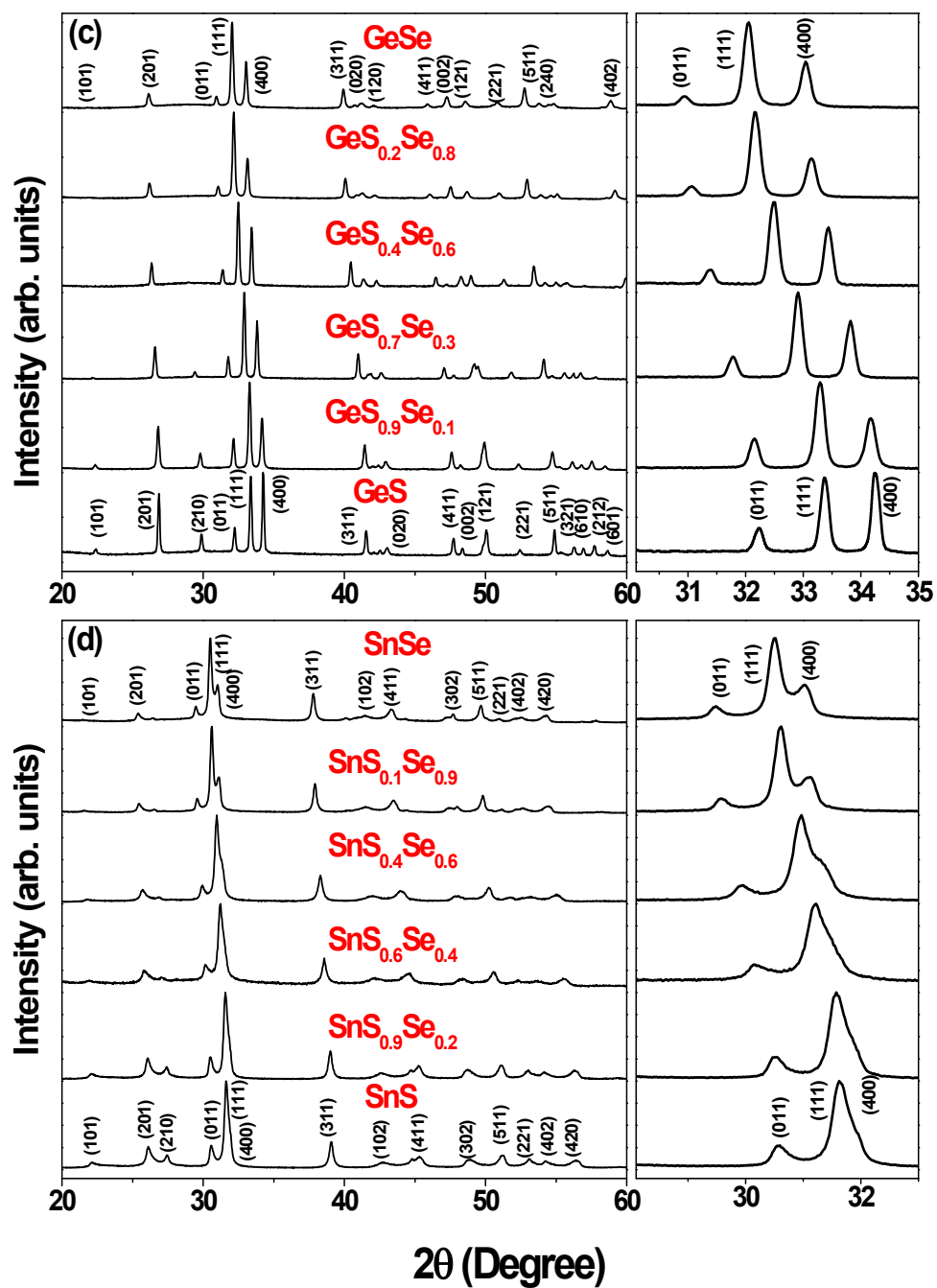
Figure S2. EDX data of $Sn_xGe_{1-x}S$ and $Sn_xGe_{1-x}Se$ NCs
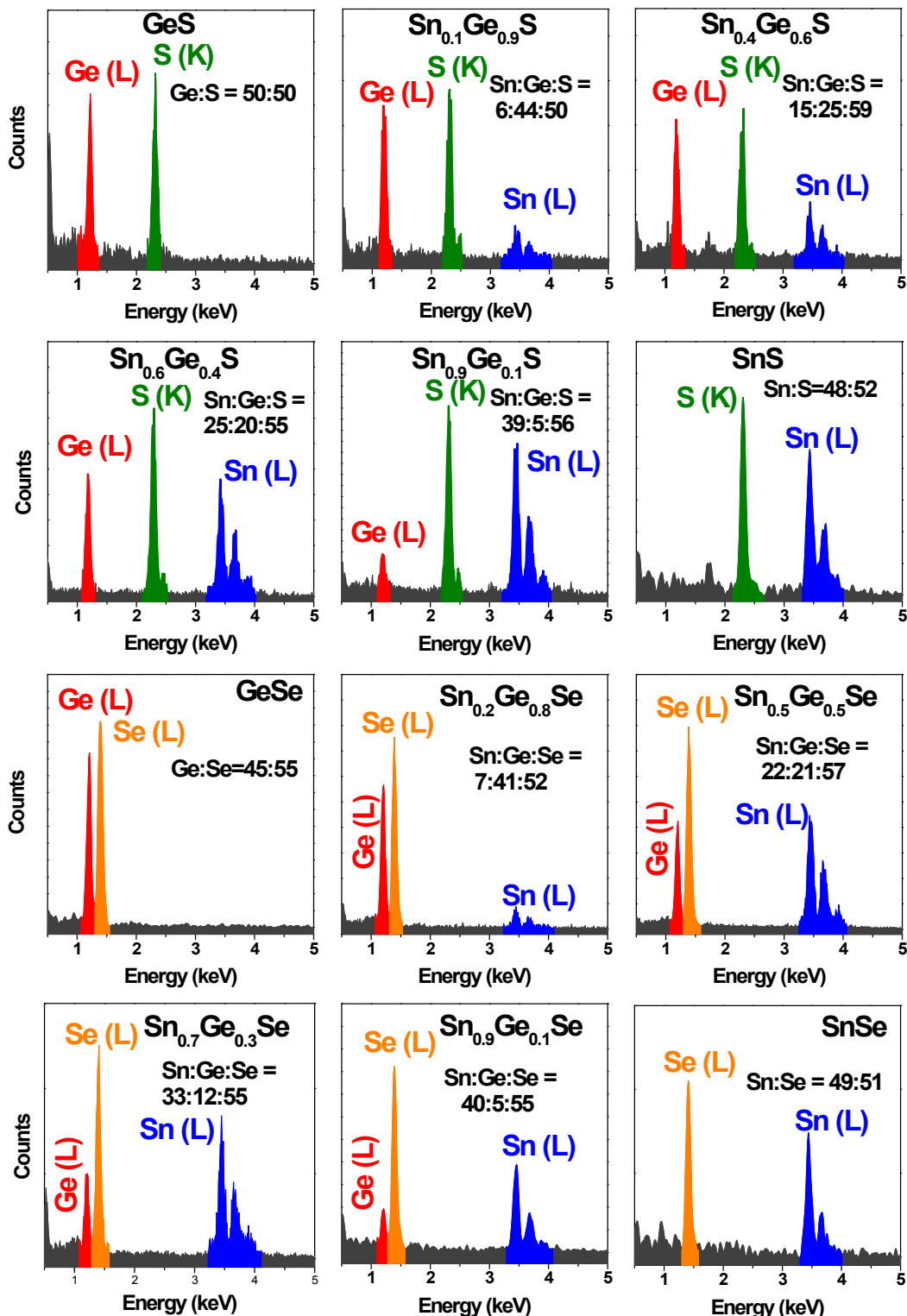
Figure S3. Correlation of EDX data of $Sn_xGe_{1-x}S$ and $Sn_xGe_{1-x}Se$ NCs with the averaged Sn composition (x) obtained from the XRD.
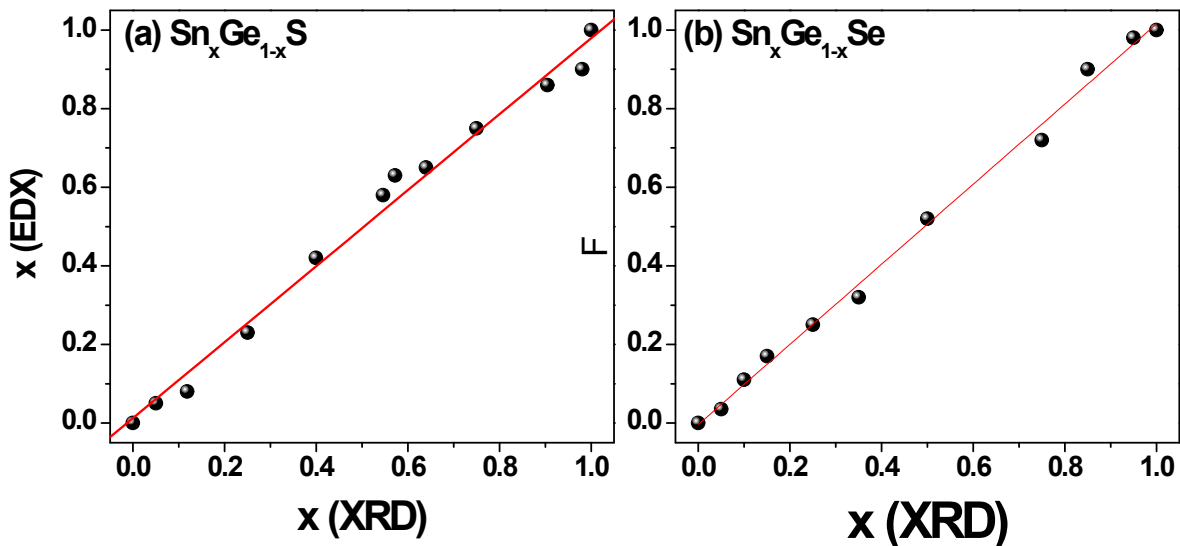
**Figure S4**. Correlation of the averaged Sn (or S) composition (x) (obtained from the XRD) and the fraction of Sn (=[TMT]/([TMG]+[TMT])) or S (=[H_2S]/([H_2S]+[DMS])) precursors in the closed reactors for (a) $Sn_xGe_{1-x}S$, (b) $Sn_xGe_{1-x}Se$, (c) GeS_xSe_{1-x}, and (d) SnS_xSe_{1-x} NCs.
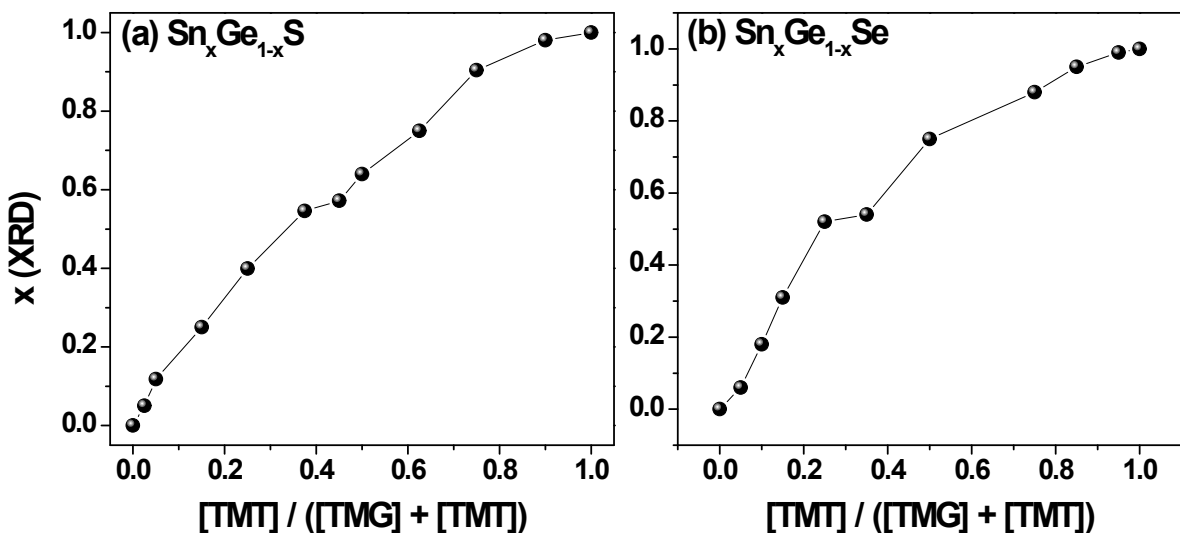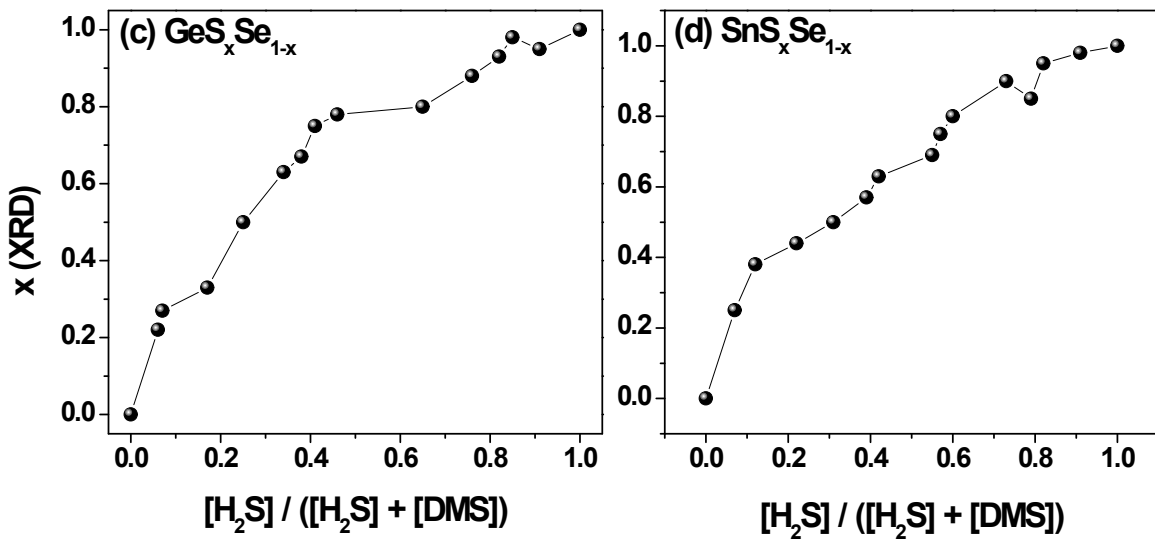
Figure S5. Raman spectrum of (a) $Sn_xGe_{1-x}S$, (b) $Sn_xGe_{1-x}Se$, (c) GeS_xSe_{1-x}, and (d) SnS_xSe_{1-x} NCs. The three peaks of GeS at 203, 232, and 260 cm^{-1} are assigned to the transverse optical (TO) modes and the broad band at 350 cm^{-1} to the longitudinal optical (LO) modes.[1,2] The peak of SnS at 309 cm^{-1}, GeSe at 202 cm^{-1}, and SnSe at 182 cm^{-1} is assigned to the LO phonon modes (B_{2g} symmetry).[3,4]

Crag reported that SnS_xSe_{2-x} followed a typical two-mode behaviors of pseudo-binary alloy throughout the composition range $0 < x < 1$; that is, there are two subbands of transverse (TO) and longitudinal (LO) optical phonons, called SnSe-like and SnS-like, respectively.[5] The two-mode behavior was also observed for the CdS_xSe_{1-x} and ZnS_xSe_{1-x}.[6] The spectrum of SnS_xSe_{1-x} shows the two-mode behavior; the SnSe-like LO phonon mode (at 182~199 cm^{-1}) is dominant in the range of $0 \leq x \leq 0.5$, whereas the SnS-like LO phonon mode (at 298~309 cm^{-1}) is dominant in the range of $0.5 \leq x < 1$. The incorporating the lighter atoms (S) leads a blue shift of the SnSe-like LO mode, while a red shift of the SnS-like LO mode. For the GeS_xSe_{1-x}, the peak of the GeSe-like LO mode shows the blue shift upon the S

incorporation. The TO modes of GeS becomes broader and shift to the lower frequency as the Se composition increases. The general feature follows the two-mode behavior.

The cation alloy show complicated behaviors, not following one-mode (e.g., $Cd_xZn_{1-x}S$ and $Cd_xZn_{1-x}Se$) or two-mode behaviors. In the $Sn_xGe_{1-x}S$, the TO modes of GeS becomes broader and shift to the lower frequency as the Sn composition increases. The LO phonon mode of SnS shows a small red shift (from 309 to 303 cm^{-1}) upon the incorporation of the ligher Ge ($0.5 \leq x \leq 1$), which is not consistent with the one-mode or two-mode behaviors. In the $Sn_xGe_{1-x}Se$, the LO phonon mode of GeSe (202 cm^{-1}) disappears and the LO phonon modes of SnSe (182 cm^{-1}) exists over short composition range ($0.8 \leq x \leq 1$). New peak appears at 210 cm^{-1} in the composition range of $0.3 \leq x \leq 0.8$.

The well-defined two-mode behaviors of the SnS_xSe_{1-x} with the large peak shift may be correlated with a homogeneous distribution of atoms over the alloy NC. More complex peak shift of the cation alloy NCs would be correlated with the less homogenous composition distribution, which causes the aniostropic change of the lattice constants.

References:

(1) Wiley, J. D.; Buekel, W. J.; Schmidt, R. L. Infrared Reflectivity and Raman Scattering in GeS. *Phys. Rev. B* **1976**, *13*, 2489-2496.

(2) Ogura, H.; Matsuishi, K.; Onari, S. Low frequency Raman Scattering of amporphous $Ge_{1-x}S$ ($0 \leq x \leq 0.62$). *Journal of Non-Crystalline Solids* **2002**, *299-302*, 973–977.

(3) Chandrasekhar, H. R.; Humphreys, R. G.; Zwick, U.; Cardona, M. Infrared and Raman Spectra of the IV-VI compounds SnS and SnSe. *Phys. Rev. B* **1977**, *15*, 2177-2183.

(4) Fukunaga, T.; Sugai, S.; Kinosada. T.; Murase, K. Observation of New Raman Lines in GeSe and SnSe at Low Temperatures. *Solid State Commun.* **1981**, *38*, 1049-1052.

(5) Chang, I. F.; Mitra, S. S. Application of a Modified Random-Element-Isodisplacement Model to Long-Wavelength Optic Phonons of Mixed Crystal. *Phys. Rev.* **1968**, *172*, 924-933.

(6) Garg, A. K. Concentration Dependent Vibrational Mode Behaviour in the Mixed Crystal System SnS$_x$Se$_{2-x}$. *Journal of Molecular Structure* **1991**, *247*, 47-60.
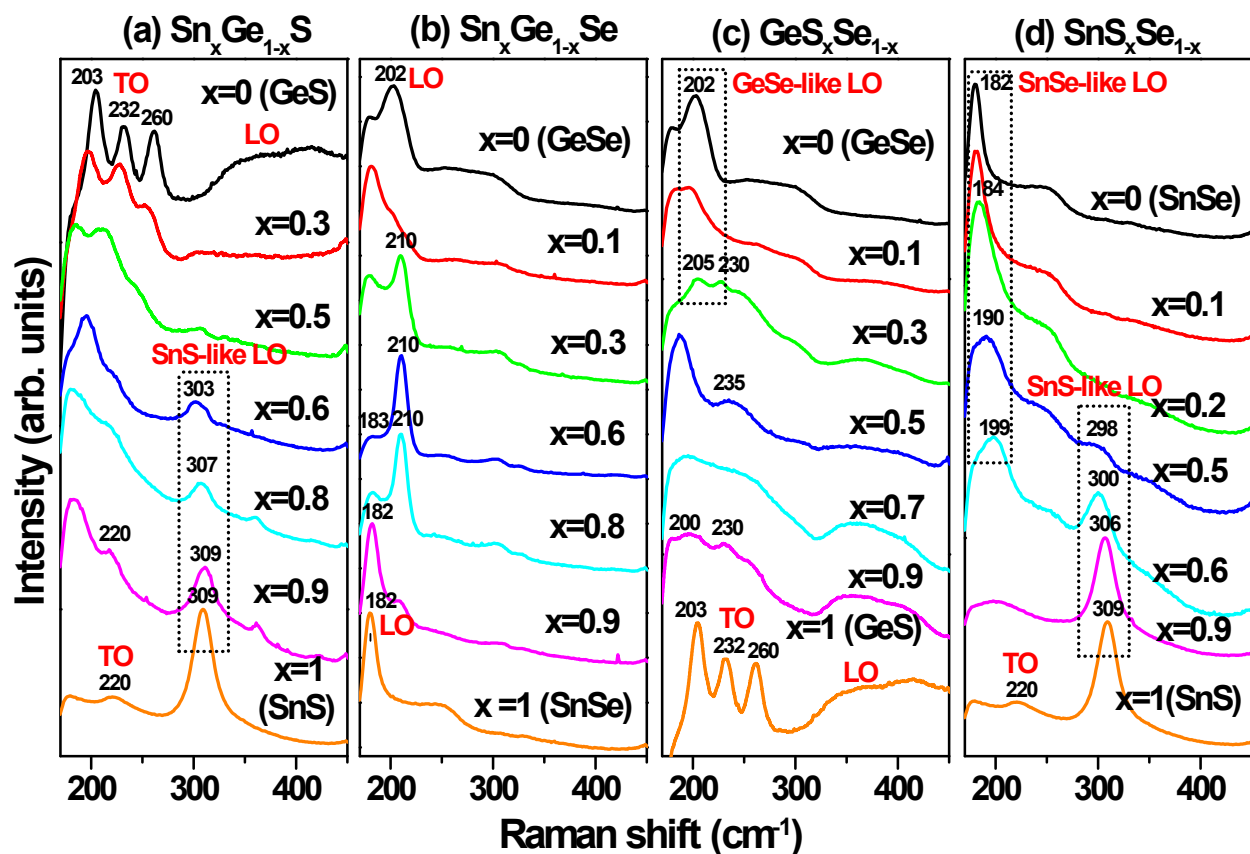
Figure S6. Plot of UV-visible-NIR diffuse reflectance spectrum and transformed Kubelka-Munk (K-M) functions, $[F(v)h\nu]^{1/2}$ and $[F(v)h\nu]^2$, where $F(v)$ is the diffuse reflectance spectrum, versus photon energy of (a) $Sn_xGe_{1-x}S$ ($x = 0, 0.1, 0.4, 0.6, 0.9$, and 1), (b) $Sn_xGe_{1-x}Se$ ($x = 0, 0.2, 0.5, 0.7, 0.9$, and 1), (c) GeS_xSe_{1-x} ($x = 0, 0.1, 0.4, 0.7, 0.9$, and 1), and (d) SnS_xSe_{1-x} ($x = 0, 0.2, 0.4, 0.6, 0.9$, and 1). The indirect and direct band gaps were estimated from the onset of $[F(v)h\nu]^{1/2}$ and $[F(v)h\nu]^2$ functions, respecticvely. The value of the onset of diffuse reflectance spectrum and indirect/diret bad gap are summarized in Table S2.

(a) $Sn_xGe_{1-x}S$

Legend:
- x=0 GeS
- x=0.1
- x=0.4
- x=0.6
- x=0.9
- x=1 SnS

(b) $Sn_xGe_{1-x}Se$

Legend:
- x=0 GeSe
- x=0.2
- x=0.5
- x=0.7
- x=0.9
- x=1 SnSe

(c) GeS_xSe_{1-x}

Legend:
- x=0 GeSe
- x=0.1
- x=0.4
- x=0.7
- x=0.9
- x=1 GeS

(d) SnS_xSe_{1-x}

Legend:
- x=0 SnSe
- x=0.2
- x=0.4
- x=0.6
- x=0.9
- x=1 SnS

Absoption (%)

$[F(R)h\nu]^{1/2}$

$[F(R)h\nu]^2$

Energy (eV)
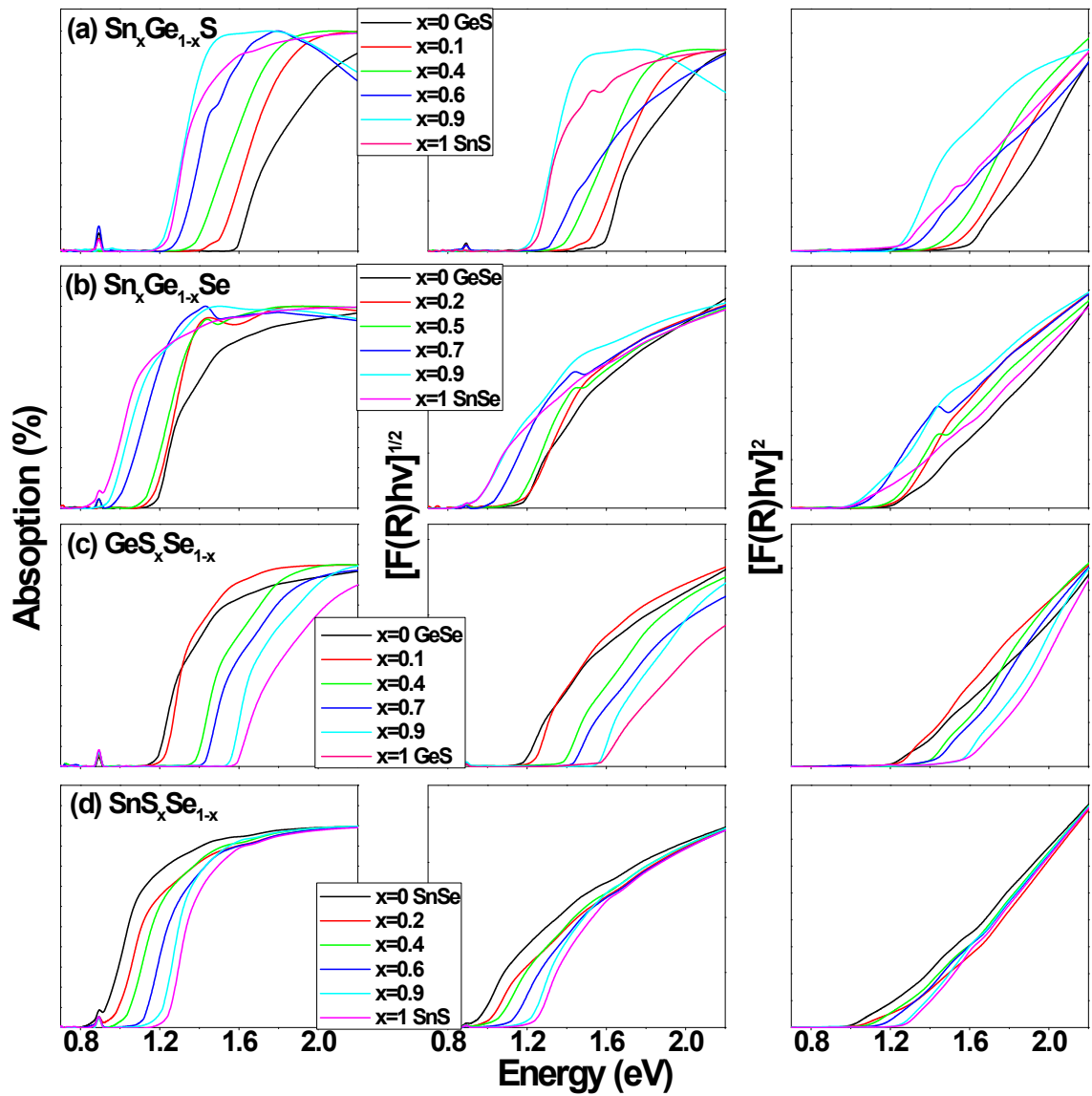
Figure S7. The CV curves of $Sn_xGe_{1-x}S$ (x = 0, 0.1, 0.4, 0.9, and 1), and $Sn_xGe_{1-x}Se$ (x = 0, 0.5, and 1), NCs were recorded at a scan rate of 20 mVs^{-1}, showing clearly the strong oxidation peaks with an onset (E_{ox}) in the range of 0.2–0.5 V, relative to the Ag/Ag$^+$ reference electrode.